Theoretical Study of the Oxidation of Alcohol to Aldehyde by d^0 Transition-Metal−Oxo Complexes: Combined Approach Based on Density Functional Theory and the Intrinsic Reaction Coordinate Method

Liqun Deng and Tom Ziegler*

Department of Chemistry, University of Calgary, Calgary, Alberta, Canada T2N 1N4

Received August 6, 1996[⊗]

A combined density functional (DF) and intrinsic reaction coordinate (IRC) method has been applied to the mechanistic study of methanol oxidization to formaldehyde by the d^0 transition-metal−oxo complexes MO_2X_2 (M = Cr, Mo, X = Cl; M = Ru, X = O). A two-step mechanism was investigated. The two steps involve addition of the methanol O−H bond to an M=O linkage to form a M−methoxy complex, $MO_2X_2 + CH_3OH = M(O)(OH)Cl_2(OCH_3)$ (step 1), and the elimination of formaldehyde from the M−methoxy complex to yield the final products, $M(O)(OH)Cl_2(OCH_3) = M(OH)_2X_2 + CH_2O$ (step 2). The calculated vibrational adiabatic intrinsic barriers were 23.7 kcal/mol (Cr), 16.2 kcal/mol (Mo), and 21.4 kcal/mol (Ru) for the addition process (1), as well as 23.1 kcal/mol (Cr), 33.3 kcal/mol (Mo), and 7.4 kcal/mol (Ru) for the elimination step (2). The enthalpies of the overall oxidation process were computed to be 3.1 kcal/mol (Cr), 41.9 kcal/mol (Mo), and −1.9 kcal/mol (Ru). The IRC trajectories revealed that reaction 1 is initiated by the formation of the weaker adduct $CH_3OH-MO_2X_2$ between the initial reactants, whereas reaction 2 results in the strong adduct $CH_2O-M(OH)_2X_2$ between final products. It is concluded that only the chromium and ruthenium oxo complexes are efficient reagents for the conversion of methanol to formaldehyde.

Downloaded by CARLI CONSORTIUM on June 30, 2009
Published on February 18, 1997 on http://pubs.acs.org | doi: 10.1021/om9606606

I. Introduction

The oxidation of alcohols to aldehydes and ketones by high-valent transition-metal (TM) oxo complexes constitutes a subject of considerable interest in organic and organometallic chemistry.[1] The first mechanistic study in this field was conducted in 1949 by Westheimer,[2] who demonstrated that the mechanism of alcohol oxidation by dioxochromium(VI) complexes involves the formation of a chromate ester. Westheimer further proposed that the chromate ester would subsequently undergo a hydride transfer from the alkoxide to a chromium metal (M) oxo group, thus eliminating either an aldehyde or a ketone as illustrated in Scheme 1. The mechanism in Scheme 1 has since then been substantiated by additional experimental investigations.[3] DuMez and Mayer[4] have most recently demonstrated that a hydride transfer mechanism similar to that of Scheme 1 is operative in processes where aldehydes are eliminated from rhenium(V) oxo alkoxide complexes. Possible structures for the transition states **TS1** and **TS2** in Scheme 1 have also been postulated. Thus, kinetic isotope effect measurements led Scott et al.[3a] to suggest that the transition state **TS2** might have a five-membered-ring structure with a partially cleaved C−H bond (Chart 1).

Scheme 1

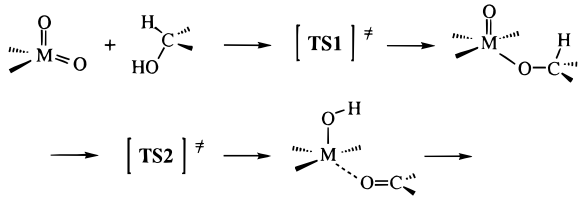

Chart 1

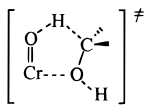

Alcohol oxidation mediated by oxometal complexes has also been investigated by computational methods.[5] Ziegler and Li[5a] explored the thermochemistry of methanol oxidation to formaldehyde by chromyl chloride (CrO_2Cl_2) in a study based on density functional theory (DFT). This investigation[5a] has more recently been extended to a systematic DFT study[6] on the thermochemistry of C−H and O−H bond activation of methanol by model d^0 oxometal complexes for all transition metals

[⊗] Abstract published in *Advance ACS Abstracts,* February 1, 1997.

(1) (a) Parshall, G. W.; Ittel, S. D. *Homogeneous Catalysis*, 2nd ed.; Wiley-Interscience: New York, 1992. (b) *Comprehensive Organic Synthesis*; Trost, B. M., Ed.; Pergamon: New York, 1991; Vol. 7 (Oxidation). (c) Nugent, W. A.; Mayer, J. M. *Metal-Ligand Multiple Bonds*; Wiley: New York, 1988. (d) *Organic Syntheses by Oxidation with Metal Compounds*; Mijs, W. J., de Jonge, C. R. H. I., Eds.; Plenum: New York, 1986. (e) Sheldon, R. A.; Kochi, J. K. *Metal-Catalyzed Oxidation of Organic Compounds*; Academic Press: New York, 1981. (f) *Oxidation in Organic Chemistry*; Wiberg, K. B., Ed.; Academic Press: New York, 1965; Part A.

(2) Westheimer, F. *Chem. Rev.* **1949**, *45*, 419.

(3) (a) Scott, S. L.; Bakac, A.; Espenson, J. H. *J. Am. Chem. Soc.* **1992**, *114*, 4205. (b) Lee, D. G.; Chen, T. *J. Org. Chem.* **1991**, *18*, 5341, and references therein. (c) Lee, D. G.; van den Engh, M. *Can. J. Chem.* **1972**, *50*, 2000. (d) Lee, D. G.; Stewart, R. *J. Org. Chem.* **1967**, *32*, 2868.

(4) DuMez, D. D.; Mayer, J. M. *Inorg. Chem.* **1995**, *34*, 6396.

(5) (a) Ziegler, T.; Li, J. *Organometallics* **1995**, *14*, 214. (b) Cundari, T. R.; Drago, R. S. *Inorg. Chem.* **1990**, *29*, 3904. (c) Rappé, A. K.; Goddard, W. A., III. *J. Am. Chem. Soc.* **1982**, *104*, 3287.

(6) Deng, L.; Ziegler, T. *Organometallics* **1996**, *15*, 3011.

S0276-7333(96)00660-7 CCC: $14.00 © 1997 American Chemical Society

Downloaded by CARLI CONSORTIUM on June 30, 2009
Published on February 18, 1997 on http://pubs.acs.org | doi: 10.1021/om9606606

(TMs) in the groups 5−8. Both investigations point to the mechanism in Scheme 1 as the thermodynamically most favorable for oxidation of methanol to formaldehyde by d^0 oxometal complexes.

We present in this account a detailed kinetic investigation of methanol oxidation by the representative transition-metal oxo species CrO_2Cl_2, MoO_2Cl_2, and RuO_4 for the two steps (eqs 1 and 2) illustrated in Scheme 1. The specific TM reagents were chosen for a

$$MO_2X_2 + CH_3OH = M(O)X_2(OH)(OCH_3) \quad (1)$$

$$M(O)X_2(OH)(OCH_3) = MX_2(OH)_2 + CH_2O \quad (2)$$

number of reasons. In the case of CrO_2Cl_2, oxidation by chromium(VI) oxo complexes has been studied extensively by experimental techniques.[1−3] On the other hand, oxo complexes of ruthenium are recognized as the most effective reagents for a selective oxidation of organic substrates, including alcohols.[1,7] Finally, the molybdenum system was included in order to get some ideas about periodic trends in the kinetic parameters within the same transition-metal triad.

It is the goal of the present investigation to extend previous thermochemical studies by providing a detailed account of the kinetic aspects of the processes outlined in Scheme 1. We shall to this end supply transition-state structures, **TS1** and **TS2** in Scheme 1, for all three reaction systems. Further, the entire reaction path will be traced by the intrinsic reaction coordinate (IRC) method in the case of $CrCl_2O_2 + CH_3OH$.

II. Computational Details

All calculations were performed using the Amsterdam Density Functional (ADF) package developed by Baerends *et al.*[8] and vectorized by Ravenek.[9] The adopted numerical integration scheme was that of te Velde *et al.*[10] A set of auxiliary s, p, d, f, and g STO functions, centered on all nuclei, were introduced in order to fit the molecular density and Coulomb potential accurately in each SCF cycle.[11] An uncontracted triple-ζ STO basis set was employed for the *n*s, *n*p, *n*d, (n + 1)s, and (n + 1)p valence orbitals of the transition-metal elements. For carbon (2s, 2p), oxygen (2s, 2p), chlorine (3s, 3p), and hydrogen (1s), use was made of a double-ζ basis set augmented by an extra polarization function.[12] The fully occupied inner shells of chlorine and chromium (1s2s2p) and molybdenum and ruthenium (1s2s2p3s3p3d), as well as carbon and oxygen (1s), were assigned to the cores and treated by the frozen-core approximation.[18] All the geometries and frequencies were calculated at the local density approximation (LDA) level[13] with the parametrization method of Vosko *et al.*[14] The relative energies were evaluated by including Becke's nonlocal exchange[15] and Perdew's nonlocal correlation[16] corrections as perturbations, NL-P, based on the LDA density. A more sophisticated approach, NL-SCF, in which the nonlocal corrections were added self-consistently,[17] was also applied for the purpose of validating the NL-P scheme. Relativistic corrections to the total energy were taken into account by first-order perturbation theory (FO).[18]

The geometry optimization procedure was based on an analytic gradient method developed by Versluis and Ziegler.[19] The harmonic vibrational frequencies were computed from the force constants obtained by numerical differentiation of the energy gradients.[20] The transition-state structures were located by a series of constraint geometry optimizations in which the bonds formed and broken were fixed at various lengths while the remaining internal coordinates were optimized. The approximate stationary points located from such a procedure were then fully optimized using the standard transition-state optimization procedure with an algorithm due to Banerjee et al. in the ADF implementation method of Fan and Ziegler.[21] The reaction pathways were traced by the intrinsic reaction coordinate (IRC) method of Fukui[22] in an algorithm developed by Gonzalez and Schlegel[23] and incorporated into the ADF program by Deng and Ziegler.[24]

III. Results and Discussion

We shall now turn to a full discussion of the reaction path for the process shown in Scheme 1. The first sections, A−E, will be devoted to the geometrical features of the stationary points and the structural changes along the reaction path. A complete discussion of the energy profile for the process shown in Scheme 1 will be given in Section F.

A. Geometries of the Reactants and Products. The molecular and electronic structure of the reactants (**1a**) and products (**2a**) in eq 1 have been studied previously.[6] We present in Figure 1 only the main structural data for these species. Also reported in Figure 1 are optimized geometries for the products of reaction 2, $CH_2O + Cr(OH)_2X_2$ (**3a**).

The oxometal species **1a** and **2a** are d^0 complexes with a singlet ground state, whereas the dihydroxymetal complex **3a** has a d^2 configuration with a triplet ground state. The optimized structures of **3a** are pseudotetrahedral with two hydrogens sticking unsymmetrically out of the O−M−O plane. Frequency calculations confirmed that the structures reported in Figure 1 all represent energy minimum points. To ensure that these conformations represent a global minimum, we also examined three other stereoisomers of the dihydroxymetal complexes in which the five atoms H−O−M−O−H are placed in a symmetry plane with three

(7) (a) Bailey, A. J.; Griffith, W. P.; Savage, P. D. *J. Chem. Soc., Dalton Trans.* **1995**, *7*, 3537. (b) Ley, S. V.; Norman, J.; Griffith, W. P.; Marsden, S. P. *Synthesis* **1994**, 639. (c) Griffith, W. P. *Chem. Soc. Rev.* **1992**, *21*, 179.
(8) Baerends, E. J.; Ellis, D. E.; Ros, P. *Chem. Phys.* **1973**, *2*, 41.
(9) Ravenek, W. In *Algorithms and Applications on Vector and Parallel Computers*; te Riele, H. J. J., Dekker, T. J., van de Vorst, H. A., Eds.; Elsevier: Amsterdam, 1987.
(10) (a) Boerrigter, P. M.; te Velde, G.; Baerends, E. J. *Int. J. Quantum Chem.* **1987**, *33*, 87. (b) te Velde, G.; Baerends, E. J. *J. Comput. Phys.* **1992**, *99*, 84.
(11) Krijn, J.; Baerends, E. J. *Fit Functions in the HFS-Methods*; Internal Report; Free University of Amsterdam: Amsterdam, The Netherlands, 1984.
(12) (a) Snijders, G. J.; Baerends, E. J.; Vernooijs, P. *At. Nucl. Data Tables* **1982**, *26*, 483. (b) Vernooijs, P.; Snijders, G. J.; Baerends, E. J. *Slater Type Basis Functions for the Whole Periodic System*; Internal Report; Free University of Amsterdam, Amsterdam, The Netherlands, 1981.
(13) Gunnarson, O.; Lundquist, I. *Phys. Rev.* **1974**, *B10*, 1319.
(14) Vosko, S. H.; Wilk, L.; Nusair, M. *Can. J. Phys.* **1980**, *58*, 1200.
(15) Becke, A. D. *Phys. Rev. A* **1988**, *38*, 2398.
(16) (a) Perdew, J. P. *Phys. Rev. Lett.* **1985**, *55*, 1655. (b) Perdew, J. P. *Phys. Rev. B* **1986**, *33*, 8822. (c) Perdew, J. P.; Wang, Y. *Phys. Rev. B* **1986,** *33*, 8800.
(17) Fan, L.; Ziegler, T. *J. Chem. Phys.* **1991**, *94*, 6057.
(18) (a) Snijders, J. G.; Baerends, E. J.; Ros, P. *Mol. Phys.* **1978**, *36*, 1789. (b) Snijders, J. G.; Baerends, E. J.; Ros, P. *Mol. Phys.* **1979**, *38*, 1909.
(19) Verluis, L.; Ziegler, T. *J. Chem. Phys.* **1988**, *88*, 322.
(20) Fan, L.; Versluis, L.; Ziegler, T.; Baerends, E. J.; Ravenek, W. *Int. J. Quantum Chem.* **1988**, *S22*, 173.
(21) (a) Banerjee, A.; Adams, N.; Simons, J.; Shepard, R. *J. Phys. Chem.* **1985**, *89*, 52. (b) Baker, J. *J. Comput. Chem.* **1986**, *7*, 385. (c) Fan, L.; Ziegler, T. *J. Chem. Phys.* **1990**, *92*, 3645.
(22) (a) Fukui, K. *J. Phys. Chem.* **1970**, *74*, 4161. (b) Fukui, K. *Acc. Chem. Res.* **1981**, *14*, 363.
(23) Gonzalez, C.; Schlegel, H. B. *J. Phys. Chem.* **1990**, *94*, 5523.
(24) (a) Deng, L.; Ziegler, T.; Fan, L. *J. Chem. Phys.* **1993**, *99*, 3823. (b) Deng, L.; Ziegler, T. *Int. J. Quantum Chem.* **1994**, *52*, 731.

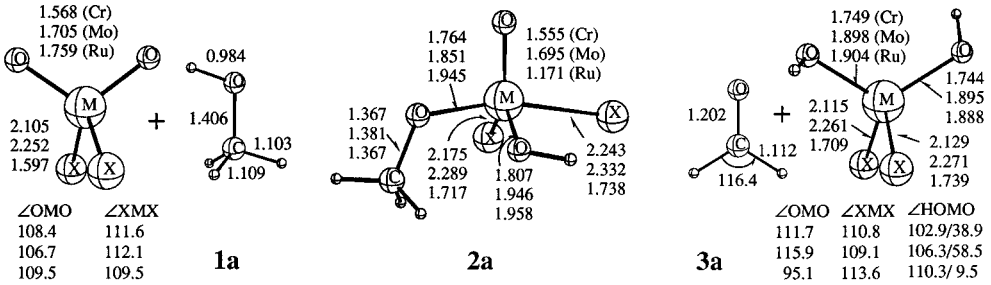

Figure 1. Geometric structures of the reactants (**1a**), intermediates (**2a**), and products (**3a**) of the methanol oxidation by the oxometal complexes MO_2Cl_2 (M = Cr, Mo, X = Cl; M = Ru, X = O).

Table 1. Geometrical Parameters for the Transition States TS1 and TS2[a]

params[b] (Å or deg)	TS1			TS2		
	Cr	Mo	Ru	Cr	Mo	Ru
a	1.556 (1.574)	1.694	1.705	1.671 (1.696)	1.845	1.782
b	1.710 (1.741)	1.827	1.852	1.774 (1.804)	1.907	1.935
c	2.025 (2.095)	2.125	2.235	1.786 (1.829)	1.897	1.988
d	2.170 (2.204)	2.295	1.723	2.109 (2.146)	2.247	1.703
e	2.135 (2.172)	2.260	1.719	2.252 (2.298)	2.331	1.750
f	1.323 (1.376)	1.258	1.316	1.395 (1.413)	1.636	1.259
g	1.117 (1.097)	1.178	1.129	1.213 (1.212)	1.089	1.397
h	1.393 (1.419)	1.399	1.373	1.311 (1.327)	1.301	1.320
i	2.059 (2.087)	2.171	2.152	2.337 (2.354)	2.414	2.526
ab	106.4 (106.4)	105.1	113.6	120.1 (121.2)	118.0	117.8
ac	108.2 (108.1)	110.2	90.1	83.5 (83.4)	78.9	80.7
ad	102.3 (102.6)	103.8	110.1	118.6 (118.1)	119.2	116.1
ae	105.3 (105.6)	106.1	109.2	88.7 (90.0)	88.6	96.1
ch	133.2 (131.1)	135.9	119.8	120.4 (120.4)	127.8	113.3
ach	114.9 (125.1)	112.0	121.8	−21.0 (−18.2)	−21.9	−30.5
cbg/agf[c]	8.8 (9.0)	6.6	4.2	14.2 (14.0)	14.3	12.0

[a] For the chromium system, the data in parentheses are the NL-SCF results. [b] See Figure 2 for a definition. [c] *cbg* for **TS1** and *agf* for **TS2**.

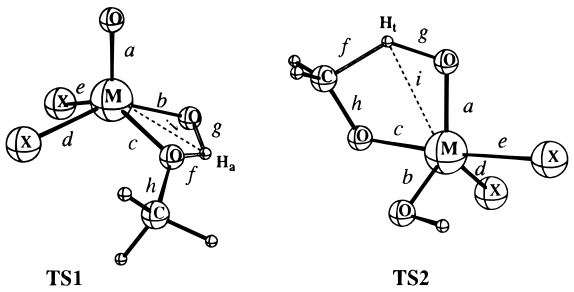

Figure 2. Definition of structural parameters in the transition states for the O−H bond addition (**TS1**) and the formaldehyde elimination (**TS2**) processes (M = Cr, Mo, X = Cl; M = Ru, X = O).

different combinations of the relative O−H bond orientations. All the isomers were found to be between 1 and 2 kcal/mol higher in energy than **3a** and proved to be saddle points by the frequency calculations.

B. Transition-State Structures. The transition state (TS) **TS1** for the [2 + 2] path of eq 1 was found to have a four-center kite structure, as depicted in Figure 2, whereas the optimized TS for step 2, **TS2**, possesses a five-membered-ring structure as suggested by Scott[3a] et al. (Figure 2). Calculations of the energy Hessians revealed a unique negative eigenvalue for each of these TSs. Table 1 contains the crucial geometric parameters for **TS1** and **TS2**. Table 2 collects the relative energies and the lowest five frequencies of the TSs. The NL-SCF geometries and relative energies of **TS1** and **TS2** for the chromium system are also compiled in Tables 1 and 2 for comparison.

As illustrated in Figure 2, the geometries of the four-center kite-shaped TSs are quite similar for chromium, molybdenum, and ruthenium. The atoms in the four-center framework are approximately coplanar, with the M−O−H−O torsion angles being 8.8 (Cr), 6.0 (Mo), and 4.2° (Ru), respectively. The distances between the activated hydrogen (H_a) and the TMs are in the range 2.05−2.17 Å (Table 1), significantly longer than the corresponding terminal hydride-metal bonds at 1.6−1.7 Å.[25] Thus, the M−H bonding interaction must be fairly weak and the mediating role of the metal in activating the O−H bond modest. This is different from the metathetical C−H activation by electron-deficient met-

Table 2. Relative Energies (kcal/mol) and Lowest Five Vibrational Frequencies (cm^{-1}) of the Transition States[a]

transition states	ΔE_e	ΔE_r	ΔZPE	ΔE_o	frequency				
TS1 Cr[b]	24.6	−0.4	−1.3	22.9	525 i	38	135	170	177
	24.0	0.2		22.9					
Mo	13.9	−0.3	−1.3	12.3	844 i	38	76	132	142
Ru	20.3	2.2	−1.6	20.9	611 i	68	161	186	239
TS2 Cr[b]	32.8	0.5	−1.8	31.5	955 i	93	110	150	168
	32.0	1.1		31.3					
Mo	30.1	2.2	−0.9	31.4	283 i	92	113	132	140
Ru	22.1	4.3	−1.5	24.9	877 i	105	158	235	280

[a] All energies relative to the separated reactants (MO_2X_2 + CH_3OH); for M = Cr, Mo X = Cl, and for M = Ru, X = O. ΔE_e = the nonrelativistic electronic energies, ΔE_r = relativistic corrections, ΔZPE = vibrational zero-point energy corrections, and ΔE_o = relative energies including ΔE_r and ΔZPE corrections. [b] In the first row, the energies calculated are by the NL-P scheme and frequencies are calculated by the LDA method. In the second row, the energies are calculated at the NL-SCF level while the ΔZPEs are taken from LDA results.

(25) Li, J.; Dickson, R. M.; Ziegler, T. *J. Am. Chem. Soc.* **1995**, *117*, 11482.

Downloaded by CARLI CONSORTIUM on June 30, 2009
Published on February 18, 1997 on http://pubs.acs.org | doi: 10.1021/om9606606

Downloaded by CARLI CONSORTIUM on June 30, 2009
Published on February 18, 1997 on http://pubs.acs.org | doi: 10.1021/om9606606

als, where the mediating role of the metal is significant[26] in the four-center transition state analogous to **TS1**.

The CH_3O-H bonds about to be broken in **TS1** are longer than the emerging MO-H bonds by 0.20 (Cr), 0.08 (Mo), and 0.19 Å (Ru), respectively, indicating a later transition state for chromium and ruthenium and a more central TS for the Mo system in step 1 of Scheme 1. The positions of the transition states are in line with Hammond's postulate, given that the addition reactions are endothermic for both chromium and ruthenium reagents and nearly thermoneutral for the molybdenum system. The energetics for the processes will be discussed in detail later.

The position of a transition state can be quantitatively described by using the progress index,[27] $\chi(Q)$, as defined in eq 3, where Q is an internal coordinate and Q_R, Q_{TS}, and Q_P are the values for Q at the reactant, transition state, and product, respectively. The index $\chi(Q)$ is a

$$\chi(Q) = \frac{Q_{TS} - Q_R}{Q_P - Q_R} \times 100\ (\%) \qquad (3)$$

measure of how far Q has moved away from Q_R at the transition state. The index is most useful for internal coordinates that vary continuously over a short interval. A good example is the M−OH bond, *b*, which has an order of 2 at the reactant and an order of 1 at the product. The index $\chi(Q)$ for *b* turned out to be 59% (Cr), 51% (Mo), and 57% (Ru), respectively, again underlining the endothermicity of the addition process.

The second step in Scheme 1 is strongly exothermic for ruthenium, moderately exothermic for chromium, and strongly endothermic for molybdenum, as discussed in detail later. These differences shape the structure of **TS2** in a now-predictable way. Thus, the $C-H_t$ bond breaking and H_t-OCr bond making for the chromium system takes place nearly synchronously in the TS region, whereas for the molybdenum system the $C-H_t$ bond breaking occurs before the H_t-OMo bond making. On the other hand, in the ruthenium system H_t-ORu bond formation is ahead of $C-H_t$ bond breaking. Consistent with this, the progress index $\chi(Q)$ for parameter *a* of Figure 2 is 58% (Cr), 75% (Mo), and 17% (Ru), respectively.

Table 2 underlines that all the TSs possess a single imaginary frequency at a high absolute value as well as a number of low-frequency bands. A normal-mode analysis suggests that the unique imaginary frequency corresponds to the reaction coordinate, whereas the low frequencies result from rotation of the methyl group in **TS1** and rotation of the O−H bond around a M−O linkage in **TS2**, as well as out-of-plane torsions of the transition-state ring structures. The low values of the frequencies reflect the fact that the potential energy surfaces (PESs) along the corresponding modes are rather flat.

Tables 1 and 2 illustrate for the chromium system the difference between including nonlocal (NL) corrections in a fully self-consistent manner (NL-SCF) and as a perturbation (NL-P). In accordance with previous experiences,[6,17,24,28] the nonlocal corrections generally elongate the metal−ligand bonds and usually have only a minor influence on bond angles. For the O−H addition step, the NL corrections bring the structures of **TS1** closer to those of the products. Table 2 illustrates further that the NL-P barriers are essentially the same (±0.3 kcal/mol) as those obtained from the more sophisticated and costly NL-SCF approach. We note further that a large number of systematic studies by our group[6,21c,24,29,30] and by many others[31] have demonstrated that the nonlocal DFT method in general affords as accurate a barrier height as any practical *ab initio* method, especially for closed-shell systems. We estimate on the basis of previous experience that the calculated activation energies are on the low side with an error of as much as 5 kcal/mol.

C. Intrinsic Reaction Path for the Chromium System. The intrinsic reaction coordinate (IRC) method affords a steepest descent path in mass-weighted Cartesian coordinates from the TS toward reactants and products. Applications[24,29,32] of the IRC method to a variety of chemical reactions have demonstrated that tracing the IRC path is instructive for a detailed understanding of the elementary reaction steps.

We present here IRC paths for the two steps of Scheme 1 in the case of the chromium system. Figure 3 plots the evolution of the relative energies and the internal coordinates for the O−H addition process. The corresponding plot for the aldehyde elimination process is given in Figure 4. The IRC parameters represent in absolute terms the length of the path from the transition state. A negative value characterize the reactant path, whereas the position on the product path is given by a positive *s* value. Also plotted in Figure 4 are the HOMO and LUMO energies along the IRC paths.

An IRC path identifies unambiguously the reactant(s) and the product(s) connected to an optimized transition state. An inspection of Figure 3 reveals that the IRC path for reaction 1 on the reactant side leads to a weak adduct between CH_3OH and CrO_2Cl_2, **1b** (Figure 7), rather than the separate species. On the product side the IRC path from **TS1** extends to the methoxy−metal complex **2b** (Figure 5), which differs from the thermodynamic product **2a** by an internal rotation around the $M-OCH_3$ bond. Likewise, the IRC path of reaction 2 connects **TS2** to another rotational isomer of the methoxy−chromium complex (**2c**; Figure 5) on the reactant side and brings **TS2** to a strong adduct, $CH_2O-Cr(OH)_2-Cl_2$ (**3b**; Figure 7), on the product side, rather than to the separate species CH_2O and $Cr(OH)_2Cl_2$. We shall

(26) (a) Cundari, T. R. *J. Am. Chem. Soc.* **1992**, *114*, 10557. (b) Cundari, T. R.; Gordon, M. S. *J. Am. Chem. Soc.* **1993**, *115*, 4210. (c) Cundari, T. R. *Organometallics* **1993**, *12*, 4971. (d) Cundari, T. R. *J. Am. Chem. Soc.* **1994**, *116*, 340. (e) Folga, E.; Woo, T. K.; Ziegler, T. In *Theoretical Aspects of Homogeneous Catalysis*; van Leeuwen, P. W. N. M., Morokuma, K., Eds.;Kluwer: Dordrecht, The Netherlands, 1995; pp 115−165. (f) Folga, E.; Ziegler, T. *Can. J. Chem.* **1992**, *70*, 333. (g) Ziegler, T.; Folga, E.; Berces, A. *J. Am. Chem. Soc.* **1993**, *115*, 636. (h) Folga, E.; Ziegler, T. *New J. Chem.* **1991**, *15*, 741.

(27) Rondan, N. G.; Houk, K. N. *J. Am. Chem. Soc.* **1985**, *107*, 2099.

(28) Ziegler, T. *Chem. Rev.* **1991**, *91*, 651.

(29) (a) Deng, L.; Ziegler, T. *J. Phys. Chem.* **1995**, *99*, 612. (b) Deng, L.; Branchadell, V.; Ziegler, T. *J. Am. Chem. Soc.* **1994**, *116*, 10645.

(30) Fan, L.; Ziegler, T. *J. Am. Chem. Soc.* **1992**, *114*, 10890.

(31) (a) Stanton, R. V.; Merz, K. M., Jr. *J. Chem. Phys.* **1993**, *100*, 434. (b) Baker, J.; Muir, M.; Andzelm, J. *J. Chem. Phys.* **1994**, *102*, 2063. (c) Serfert, G.; Früger, K. In *The Reaction Path in Chemistry: Current Approaches and Perspectives*; Kluwer: Dordrecht, The Netherlands, 1995. (d) Abashkin, Y.; Russo, N.; Sicilia, E.; Toscano, M. In *Modern Density Functional Theory: A Tool for Chemistry*; Seminario, J. M, Politzer, J. M., Eds.; Elsevier: Amsterdam, 1995; Theoretical and Computational Chemistry, Vol. 2.

(32) Jensen, V. R.; Børve, K. J.; Ystenes, M. *J. Am. Chem. Soc.* **1995**, *117*, 4109.

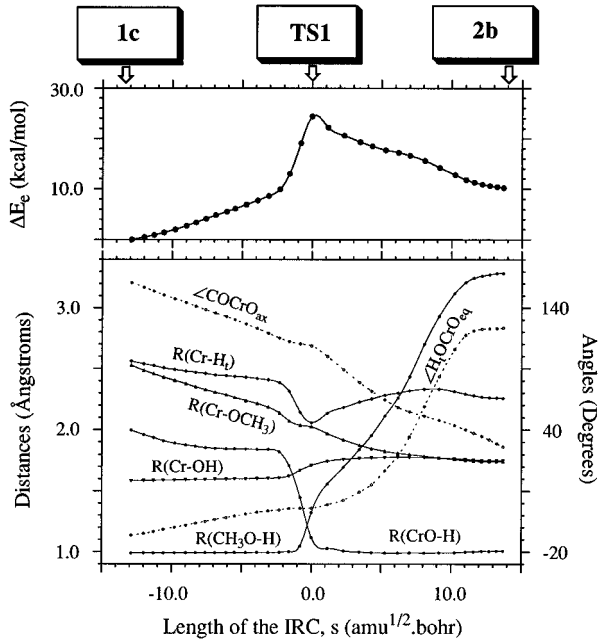

Figure 3. Electronic enthalpy, ΔE_e (relative to $CrO_2Cl_2 + CH_3OH$), and the internal coordinates of the O−H bond addition as functions of the IRC length.

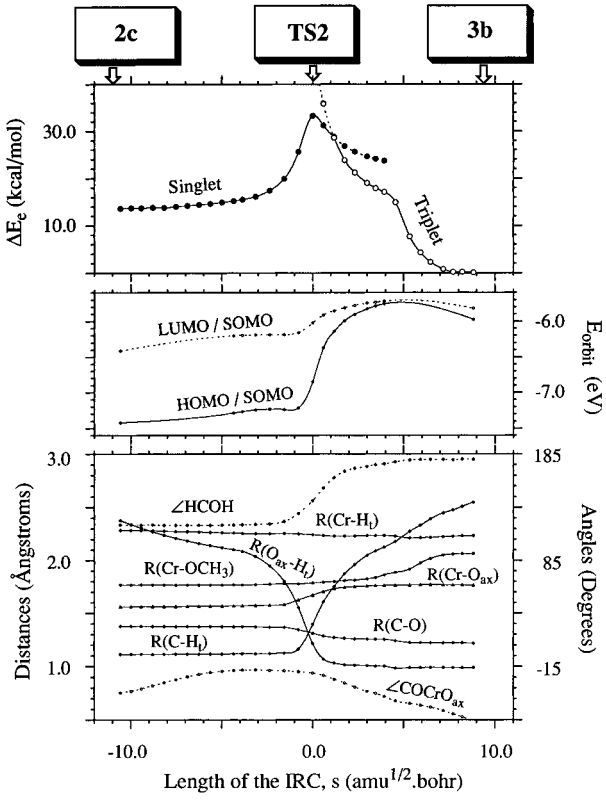

Figure 4. Electronic enthalpy, ΔE_e (relative to $CrO_2Cl_2 + CH_3OH$), HOMO/LUMO orbital energies, and the internal coordinates of reaction 2 as functions of the IRC length.

now turn to a detailed discussion of the geometrical changes along the IRC paths.

It follows from Figure 3 that reaction 1 proceeds in three stages. First, from the reactants ($s < -12$) to within the vicinity ($s = -1.5$) of **TS1**, methanol initially attacks the Cr═O linkage with the CH_3O−H bond approaching in a coplanar fashion (∠HOCrO = −18°; Figure 3) from the O−Cl−O face. The methanol molecule orients itself with an oxygen lone pair orbital

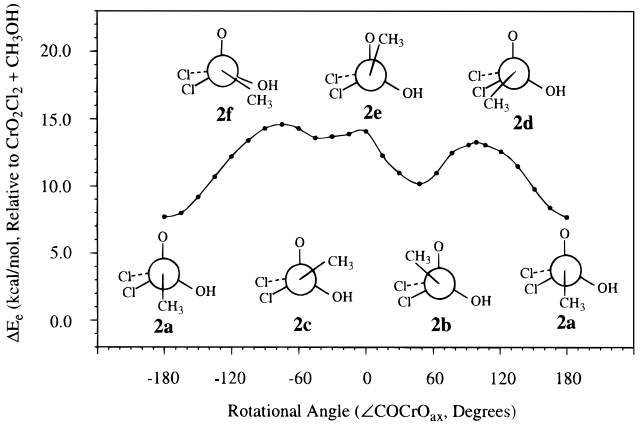

Figure 5. Energy profile of $Cl_2OCr(OH)OCH_3$ as a function of the rotational angle $\angle COCrO_{ax}$.

pointing toward the empty metal-based d orbitals so as to facilitate the donation of electron density from oxygen to the metal center. The migrating hydrogen H_a, on the other hand, is directed toward one terminal oxygen of the complex. At this stage, all geometric parameters as well as the energy in Figure 3 change gradually in a near-linear fashion. In particular, the Cr−O distance of the emerging Cr−OCH_3 bond decreases gradually while the distance between H_a and the attacked terminal oxygen is simultaneously shortened. A close inspection of Figure 3 reveals further that the M═O linkage expands slightly while the length of the CH_3O−H bond remains virtually unchanged. Thus, in the first stage the M═O bond is weakened by donation of density from the methanol oxygen lone pair into the metal-based d orbitals, which are weakly antibonding with respect to the oxygen ligands. At the same time no back-donation from the metal d orbital to the $\sigma^*(CH_3O-H)$ orbital causes the CH_3O−H bond to expand.

The second stage occurs in the TS region, where bond making and bond breaking take place in a concerted fashion, although the MO−H σ-bond formation is slightly ahead of the CH_3O−H σ-bond breaking and Cr═O π-bond elimination. As illustrated in Figure 3, from $s \approx -2.3$ to 1.2, the distance between the migrating hydrogen and the attacked terminal oxygen $R(H_a-OM)$ drops sharply from 1.82 Å to 1.03 Å, indicating that the CrO−H bond is essentially formed in this region. At the same time the CH_3O−H bond is seen to lengthen suddenly from $s \approx -1.6$ to 2.3, as $R(CH_3O-H)$ increases from 1.01 to 1.70 Å. The M═O linkage is elongated synchronously from a M═O double bond ($R(M{=}O) \approx$ 1.62 Å) to a M−OH single bond ($R(M-OH) \approx 1.76$ Å). The energy changes sharply in this region, which accounts for the barrier of the reaction.

The last stage, $s = 2-12$, can be described as the rotation of the Cr−OCH_3 and M−OH bonds out of their coplanar position from the four-center transition state so as to alleviate steric repulsion. The rotation serves further to maximize the overlap between the lone-pair p_π orbital of the methoxy oxygen and the metal d_π orbital in order to form a partial M−OCH_3 π-bond.[6] The formation of the π-bond gives rise to a gradual shortening of the M−OCH_3 linkage (Figure 3) in the region $s = 2-12$. The IRC finally terminates at the local minimum **2b,** which is about 2 kcal/mol higher in energy than the thermodynamic product **2a** (Figure 5).

Downloaded by CARLI CONSORTIUM on June 30, 2009
Published on February 18, 1997 on http://pubs.acs.org | doi: 10.1021/om9606606

Downloaded by CARLI CONSORTIUM on June 30, 2009
Published on February 18, 1997 on http://pubs.acs.org | doi: 10.1021/om9606606

We notice from Figure 3 that, during the whole reaction process, the dihedral angle ∠COCrO varies linearly from 157 to 49° in order for the two sp^3 orbitals on the methanol oxygen to maintain optimal interactions to, respectively, the migrating hydrogen and the metal d_σ orbital. These interactions are crucial for lowering the energy of the four-center kite-shaped transition state **TS1**. It is also evident that the R(Cr−H_a) distance reaches its minimum value of 2.059 Å at the TS. As discussed previously, this value is far longer than that of a normal Cr-H bond distance (about 1.6 Å). Thus, the metal center is only in part able to stabilize the hydrogen during the migration. Finally, it follows from Figure 3 that the energy profile has the typical shape of an endothermic reaction; i.e., the energy ascends steadily from the reactants to a point before the TS, increases sharply to the maximum at the TS region, and then descends smoothly from the TS to the products.

For reaction 2, as discussed previously, the reactant and TS are situated on a singlet PES while the product lies on a triplet PES. Thus, the reaction path of lowest energy involves a crossover from the singlet surface to the triplet surface. The IRC was traced on the singlet PES in the first place, since the TS is situated here. The triplet energies were calculated at each IRC point from the TS toward the product until a crossing point was found at $s = 1.2$, where the singlet-triplet energy splitting is less than 0.1 kcal/mol. From this point, the true IRC was approximately represented by the steepest descent path on the triplet PES down to the product in the mass-weighted Cartesian coordinate system. Conceptually, such a crossing would be made possible by spin−orbit coupling. As illustrated in Figure 4, tracing the IRC path on the ground-state PES for reaction 2 reveals that **TS2** on the reactant side connects to a local minimum, **2c**, which is a rotamer of the thermodynamic product **2a** and the kinetic product **2b** of reaction 1 (see Figure 6). On the product side, the reaction path links **TS2** to the adduct CH_2O−$Cr(OH)_2Cl_2$ (**3b**). The reactant **2c** and the transition state **TS2** both have an electronic singlet ground state in accordance with the formal d^0 configuration on the metal center. However, the metal center in the CH_2O−$Cr(OH)_2Cl_2$ adduct is reduced to a d^2 configuration and **3b** has a triplet ground state, as does the $Cr(OH)_2Cl_2$ complex after complete elimination of CH_2O (Figure 4).

The complicated electronic nature of the elimination process can be analyzed from the correlation diagram of Figure 6. Reaction 2 involves two electron pairs. They reside on the reactant side to the left of Figure 6 in a C−H_t σ-bonding orbital (12a) on the methoxy group as well as an oxygen lone pair (16a) on the Cr=O_{ax} linkage. Above these orbitals are the empty $d_\perp$ (28a) and $d_{||}$ (29a) components of the d^0 configuration on chromium. As the reaction proceeds, the oxygen lone pair is stabilized by the formation of the CrO_{ax}−H_t bond (14a), whereas the electron pair in the C−H_t σ-bonding orbital is destabilized as the C−H_t bond is broken. Eventually, the C−H_t σ-bonding orbital rises above the $d_\perp$ and $d_{||}$ components as it is transformed into the π^*_{CO} orbital (29a) of the H_2CO unit. At this point the d^2 configuration emerges and the triplet surface drops below that of the singlet (Figure 4). Near the crossing point the HOMO and LUMO are close in energy (Figures 4 and 6). Also, at the product side $d_{||}$ is to some degree stabilized by an interaction with the π^*_{CO} orbital 27a, corresponding to a metal to carbonyl back-donation. We shall now discuss the geometrical changes as the reaction moves from reactant to product. In this discussion we will stay on the surface of lowest energy.

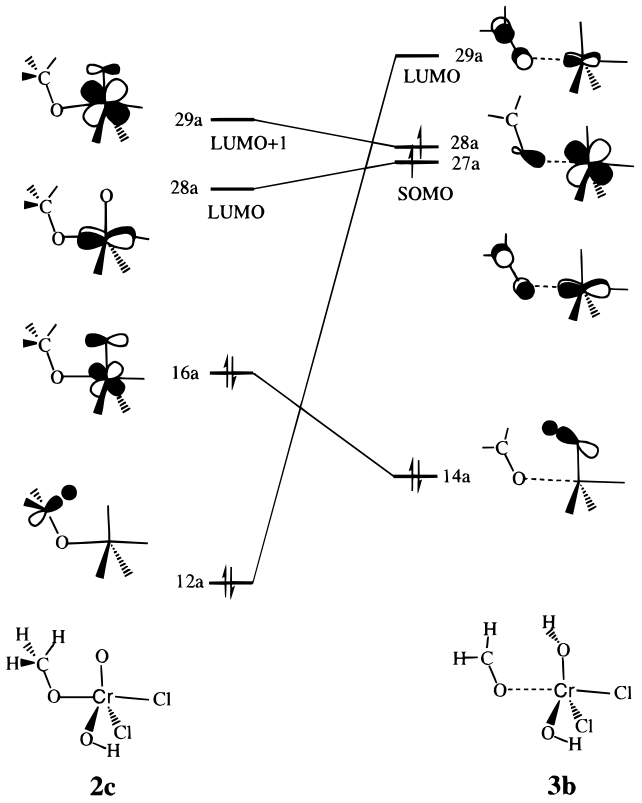

Figure 6. Correlation diagram for the formaldehyde elimination process.

The evolution of the geometrical parameters along the IRC in Figure 4 clearly indicates that the reaction has three distinct parts. In the first part from $s \approx -12$ (**2c**) to $s \approx -2$ near the TS region, the most noticeable changes in the geometry are (i) the rotation of the methoxy group around the Cr−OCH_3 bond and (ii) a contraction of the distances between the transannular hydrogen H_t and the attacked terminal oxygen O_{ax}. Thus, the dihedral angle ∠COCrO_{ax} changes from −45° to about 0°, and concurrently the R(O_{ax}−H_t) distance declines from about 2.4 to 1.8 Å, while little change is found in the other structural parameters at this stage. Evidently, the planar five-membered ring of the activated complex is forming without breaking any bonds in the system. As a result, the energy rises only slightly, mostly due to the hindered rotation around the Cr−OCH_3 bond.

The region around **TS2** from $s \approx -2$ to $s \approx 1.2$ (the crossing point) is the part of the elimination path where most changes take place (Figure 4). In this area, the emerging H_t−O_{ax} bond shortens sharply from about 1.8 to 1.0 Å, whereas the C−H_t bond about to be broken lengthens dramatically from 1.1 to 1.8 Å. Meanwhile, the R(Cr−O_{ax}) distance increases linearly from a double Cr=O bond length of 1.56 Å to the Cr−OH single-bond distance of 1.75 Å and the R(C−O) distance shrinks from the length of the H_3C−O single bond near 1.40 Å to the H_2C=O double-bond length of 1.25 Å. Furthermore, the dihedral angle of the methylene, ∠HCOH,

increases monotonically from 120 to 175°, implying rehybridization of the carbon from sp^3 in the methoxy group to sp^2 in formaldehyde. All these changes take place at the same time (Figure 4). Notice that in the vicinity of **TS2** ($s \approx 0$) the $R(C-H_t)$ and $R(CrO-H_t)$ bonds have the same length at about 1.3 Å and the $R(C-O)$ and $R(Cr-O_{ax})$ distances take the mean value of their single- and double-bond lengths, respectively.

The reaction coordinate at $s = 0$ is represented by a contraction of the $CrO-H_t$ bond and a stretch of the $C-H_t$ linkage. The associated imaginary frequency has a large absolute value (Table 2), since both bonds only are broken in part. The curvature around $s = 0$ is as a consequence large, and the energy profile reveals a narrow and sharp barrier typical for this type of tight transition state. The triplet surface comes down below the singlet surface at the last part of the second stage at $s = 1.2$. At this point, $Cr-O_{ax}H_t$ is a single bond with $R(Cr-O_{ax}) = 1.76$ Å, while $R(C-O)$ at 1.28 Å is close to the double-bond length of $H_2C{=}O$; $R(O-H_t) = 1.07$ Å is only slightly longer than the $MO-H_t$ bond of the product. Thus, the aldehyde adduct product has emerged. The crossing is characterized by a near-degeneracy of the former HOMO and LUMO from the singlet surface. We shall discuss their identity later.

The last stage ($s \geq 1.2$) of the reaction path takes place on the triplet surface. Here the motion of the H_t and the H_2CO subunits serves to relieve steric repulsion among the ligands in $Cr(OH)_2Cl_2$ and to gain better bonding interaction between H_2CO and $Cr(OH)_2Cl_2$ in the $H_2CO-Cr(OH)_2Cl_2$ adduct (**3b**). This adduct has a stabilization energy of 7.9 kcal/mol compared to the separated products, $H_2CO + Cr(OH)_2Cl_2$ (Figure 4).

We should in this section finally point out that use of the adiabatic assumption has been made in tracing the reaction path for the formaldehyde elimination process. Under this assumption, the electron wave function can change instantaneously for every change in nuclear positions so that the reaction system tends to stay on the ground-state PES. As indicated in Figure 4, the energy difference between the singlet and triplet products is as large as 25 kcal/mol, which ensures the validation of using the adiabatic assumption.

D. Internal Rotation of the Methoxy Group around the M−OCH$_3$ Bond. The IRC analyses described above suggest that steps 1 and 2 in Scheme 1 are connected by a rotation of the methoxy group in $Cr(O)Cl_2(OCH_3)$ around the $Cr-OCH_3$ bond, leading from the end point **2b** of step 1 to the starting point **2c** of step 2 (Figures 3 and 4). We have investigated the energy profile for the rotation of the methoxy group in $Cr(O)Cl_2(OCH_3)$ around the $Cr-OCH_3$ bond (Figure 5). The profile in Figure 5 was obtained by changing $\angle COCrO_{ax}$ from 0 to 360° in 25 steps, while for each point all other degrees of freedom were optimized. The rotational PES has three energy minimum points, **2a**−**c**, separated by three TSs. The two local minima correspond to the IRC end points **2b** of reaction 1 and **2c** of reaction 2, whereas the global minimum of the rotation, **2a**, represents the thermodynamic product of reaction 1, i.e., the most stable conformation of the $Cr(O)Cl_2(OH)(OCH_3)$ complex. At the three rotational TSs, the $MO-CH_3$ bond eclipses with the Cr−OH, Cr=O, and Cr−Cl bonds, respectively, whereas the three energy minimum points are the corresponding staggered

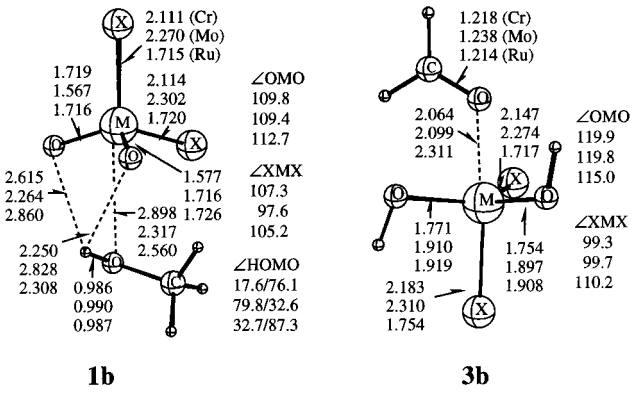

1b **3b**

Figure 7. Geometric structures of the adducts $CH_3OH-MO_2X_2$ (**1b**) and $CHO-M(OH)X_2$ (**3b**) (M = Cr, Mo, X = Cl; M = Ru, X = O).

conformations. It can be deduced from Figure 5 that the electronic energies of **2b** and **2c** are 2.2 and 5.6 kcal/mol above **2a** and that the rational barriers from **2b** to **2c** and **2a** are respectively 3.9 and 3.0 kcal/mol. The important point inferred from Figure 5 is that the rotational barriers are much lower than the barriers of reactions 1 and 2. Thus, the internal rotation process is not the rate-determining step of Scheme 1.

E. Adducts between the Organic Substrates and the Metal Complexes. The oxidation process in Scheme 1 is characterized by the formation of the adduct $CH_3OH-MO_2X_2$ (**1b**) between the two reagents at the beginning and the generation of the adduct $CH_2O-M(OH)_2X_2$ (**3b**) between the products at the end. The optimized geometries of **1b** and **3b** are shown for chromium, molybdenum, and ruthenium in Figure 7. Methanol is only bound weakly in **1b** through a donation of electron density from the methanol oxygen to the metal center. The adduct formation energies are respectively 0.8, 3.9, and 0.5 kcal/mol for the Cr, Mo, and Ru systems. The molybdenum system has the strongest adduct formation energy and the shortest $M-O(H)CH_3$ distance (Figure 7), since $MoCl_2O_2$ is best suited to coordinate a fifth ligand without steric congestion on account of the longer M=O and M−Cl distances.

The complexation energies in $CH_2O-M(OH)_2X_2$ (**3b**) are 7.9, 17.9, and 8.2 kcal/mol for Cr, Mo, and Ru, respectively, and thus are stronger than in **1b**. The aldehyde is bound to the metal center by donation from the oxygen lone pair of CH_2O to $d_{\|}$ on the metal center (28a on the right-hand side of Figure 6), as well as back-donation from $d_\perp$ to π^*_{CO}, (27a on the right-hand of Figure 6). An analysis based on the extended transition state (ETS)[33] method revealed that the stronger complexation energy in the case of molybdenum comes from the back-donation (27a on the right-hand side of Figure 6). As discussed previously,[6] the $d_\perp$ component is destabilized by antibonding interaction with the occupied p_π orbitals on the X and OH ligands of the $M(OH)_2X_2$ fragment. The stabilization increases from left to right in a transition series and from top to bottom in a triad with the radial extension of the d orbital. Thus, $d_\perp$ for molybdenum is highest in energy and most likely to back-donate.

F. Comparison of the Energy Profiles and Reaction Mechanism for the Cr, Mo, and Ru Systems.

(33) (a) Ziegler, T.; Rauk, A. *Theor. Chim. Acta* **1977**, *46*, 1. (b) Ziegler, T. *NATO ASI Ser.* **1992**, *C378*, 367.

Downloaded by CARLI CONSORTIUM on June 30, 2009
Published on February 18, 1997 on http://pubs.acs.org | doi: 10.1021/om9606606

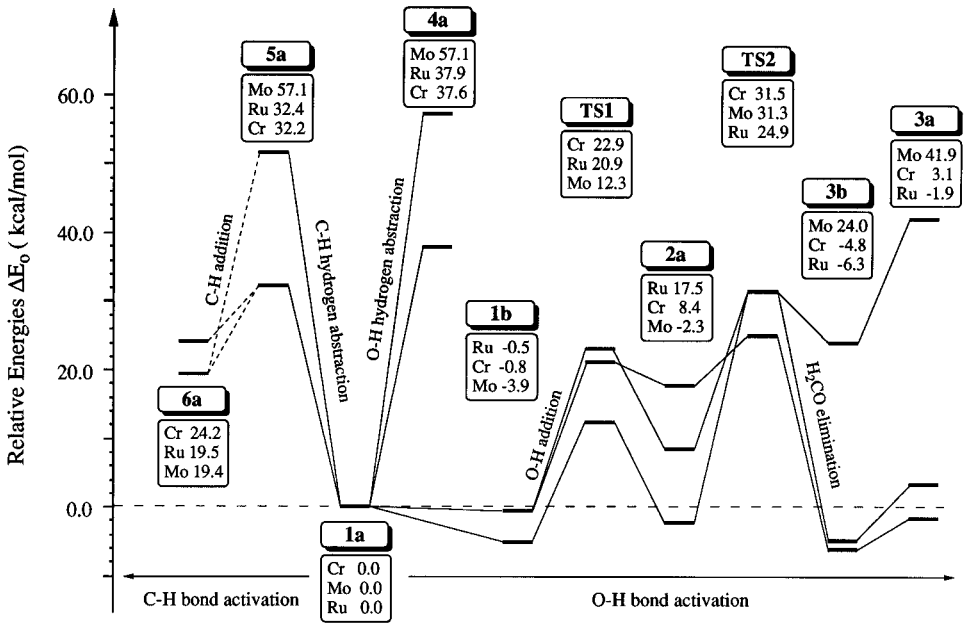

Figure 8. Vibrational adiabatic potential energy surface for the methanol oxidation by MO_2X_2 (M = Cr, Mo, X = Cl; M = Ru, X = O). ΔE_o is given relative to **1a**. Definitions: **1a**, $MO_2X_2 + CH_3OH$; **1b**, the adducts $CH_3OH-MO_2X_2$; **2a**, the most stable conformation of the complexes $M(O)Cl_2(OH)(OCH_3)$; **3a**, the final products $M(OH)_2X_2 + CH_2O$; **3b**, the $CH_2O-M(OH)_2X_2$ adducts; **4a**, $M(O)(OH)X_2 + OCH_3$; **5a**, $M(O)(OH)X_2 + CH_2OH$; **6a**, $M(O)(OH)X_2(CH_2OH)$ complexes.

Figure 8 presents the vibrational adiabatic energy profile (zero-point energy corrections included) for the oxidation of methanol to formaldehyde by the O−H addition mechanism (Scheme 1) for M = Cr, Mo, Ru.

Starting with the chromium system, we note that the calculated activation barriers for the two steps in Scheme 1 are $\Delta E^{\ddagger}_1 = 23.7$ kcal/mol and $\Delta E^{\ddagger}_2 = 23.1$ kcal/mol, respectively, whereas the overall heat of reaction leading to H_2CO and $CrCl_2(OH)_2$ is 3.1 kcal/mol. Thus, oxidation of methanol by $CrCl_2O_2$ according to Scheme 1 is feasible from both kinetic and thermochemical points of view. We note further that alcohols with deuterated C−H bonds exhibit a positive kinetic isotope effect when oxidized to aldehydes.[3] This is consistent with the high barrier of the second step as well as the partial C−H bond breakage in the tight five-membered transition state **TS2**.

The corresponding activation energies for the homologous molybdenum system are $\Delta E^{\ddagger}_1 = 16.2$ kcal/mol and $\Delta E^{\ddagger}_2 = 33.6$ kcal/mol, respectively, whereas the overall heat of reaction leading to H_2CO and $MoCl_2(OH)_2$ is 41.9 kcal/mol. Thus, $MoCl_2O_2$ is not likely to oxidize alcohols to aldehydes by the mechanism in Scheme 1. The process in Scheme 1 involves a formal reduction of the metal center by two electrons. The high overall heat of reaction for molybdenum stems from the fact that the two d-based orbitals, 27a and 28a of Figure 7, housing these electrons are strongly antibonding in the case of $MoCl_2(OH)_2$, as mentioned before. The strongly antibonding nature of the d-based orbitals is also responsible for the favorable thermochemistry and kinetics of the first step in Scheme 1 for molybdenum. This follows from the discussion given in our previous study.[6] The trend is ultimately determined by the energy of the antibonding and metal-based SOMOs (27a and 28a in Figure 7) and, in turn, by the radial extension of the metal d orbitals. Thus, the more diffuse the d orbitals, the higher the energy of the SOMOs, the stronger the $M-OCH_3$ and $M-CH_2OH$ bonds, and the weaker the MO−H bonds. This is so because the formation of the $M-OCH_3$ or $M-CH_2OH$ bonds involves the transfer of one electron from the SOMO to a low-lying ligand-based orbital, whereas the formation of a MO−H bond formally involves the promotion of one electron from the H atom to the SOMO.[6]

We finally have for ruthenium that the activation energies are $\Delta E^{\ddagger}_1 = 21.4$ kcal/mol and $\Delta E^{\ddagger}_2 = 7.3$ kcal/mol, respectively, whereas the overall heat of reaction leading to H_2CO and $RuO_2(OH)_2$ is −1.9 kcal/mol. The oxidation of alcohols by RuO_4 according to the mechanism in Scheme 1 is certainly feasible. The more compact d orbitals on ruthenium form less antibonding orbitals than do those of molybdenum in the d^0 and d^2 systems. For this reason, step 1 is most favorable for molybdenum, whereas step 2 is more feasible for ruthenium.[6]

We have so far assumed that the initial step in the alcohol oxidation involves O−H addition. Alternatively, one might imagine the C−H addition step

$$MO_2X_2 + CH_3OH \rightarrow M(O)X_2(OH)(CH_2OH) \quad (4)$$

or the abstraction of hydrogen from the C−H

$$MO_2X_2 + CH_3OH \rightarrow M(O)X_2(OH) + CH_2OH \quad (5)$$

or O−H

$$MO_2X_2 + CH_3OH \rightarrow M(O)X_2(OH) + CH_3O \quad (6)$$

bonds.

The structural and thermodynamic properties of the processes in eqs 4−6 have been reported previously.[6] For the purpose of comparison, the heats of reaction for these processes are illustrated at the left-hand side of Figure 8. The abstraction reactions have high thermodynamic energies with essentially no additional kinetic activation barriers. The abstraction reactions are not

Downloaded by CARLI CONSORTIUM on June 30, 2009
Published on February 18, 1997 on http://pubs.acs.org | doi: 10.1021/om9606606

likely to be operative in alcohol oxidation by oxo complexes.[6]

The C—H addition step has a higher reaction enthalpy than the corresponding O—H addition reaction. However, it might be operative for RuO_4 or oxo complexes of other later transition metals. We intend to investigate this path fully in a later study.

IV. Conclusions

We have used a combined DFT and IRC method to study methanol oxidation to formaldehyde by oxometal complexes. The two-step reaction pathway we probed consisted of O—H addition to a metal−oxygen bond followed by intramolecular hydrogen transfer from the methoxy group to another terminal oxygen in the M═O linkage (Scheme 1).

The IRC calculations revealed that the process in Scheme 1 in fact involves five steps. They include (i) formation of the weak adduct $CH_2OH-MO_2X_2$ (**1b**), (ii) addition of the O—H bond to a M═O linkage to yield a kinetic product of eq 1, **2b**, (iii) isomerization of **2b** to **2c** by an internal rotation of the OCH_3 group around the $M-OCH_3$ bond, (iv) transformation of a hydrogen from the methoxy group to the cis terminal oxygen of another M═O linkage to form an adduct, $CH_2O-M(OH)_2X_2$, and (v) decomposition of the adduct to yield the products $M(OH)_2X_2 + CH_2O$.

The oxidation of methanol by the mechanism given in Scheme 1 was found to be feasible for the ruthenium and chromium systems but not for $MoCl_2O_2$. The different behavior of the oxo complexes was rationalized in terms of variations in the radial extent of the d orbitals on the metal centers.

Acknowledgment. This investigation was supported by the Natural Sciences and Engineering Research Council of Canada (NSERC) as well as the donors of the Petroleum Research Fund, administered by the American Chemical Society. T.Z. thanks the Canada Council for a Killam Research Fellowship.

OM9606606

Downloaded by CARLI CONSORTIUM on June 30, 2009
Published on February 18, 1997 on http://pubs.acs.org | doi: 10.1021/om9606606